NMR features of a decagonal $Al_{72.6}Ni_{10.5}Co_{16.9}$ quasicrystal

P. Jeglič and J. Dolinšek
J. Stefan Institute, University of Ljubljana, Jamova 39, SI-1000 Ljubljana, Slovenia
(Received 20 October 2003; revised manuscript received 13 October 2004; published 14 January 2005)

The nuclear magnetic resonance (NMR) spectra of a decagonal $Al_{72.6}Ni_{10.5}Co_{16.9}$ single-grain quasicrystal (QC) were investigated by field- and frequency-sweep techniques in two magnetic fields and the ^{27}Al relaxation rate was determined. The spectra are strongly inhomogeneously broadened by the electric quadrupole interaction, as evident from the magnetic-field independence of the width of the satellite part of the spectrum and the inverse-field dependence of the width of the central line. The temperature-independent ^{27}Al isotropic Knight shift is anomalously low similarly to icosahedral Al-based QCs, whereas the line broadening due to anisotropic Knight shift is minute as compared to the quadrupolar broadening. The ^{59}Co resonance was found centered at its Larmor frequency and its temperature-independent frequency shift demonstrates that cobalt is in a nonmagnetic state. The NMR spectra exhibit orientation dependence in a magnetic field. In the twofold rotation pattern, the satellite intensity shows a pronounced orientation-dependent shape and structure, whereas this was not detected in the tenfold pattern. The tenfold rotation pattern of the ^{27}Al central line, obtained with the Fourier-transform technique, exhibits a tiny, but significant orientation dependence of the line shape and its center of gravity M_1 with the quasiperiodic symmetry $\pi/5$. The orientation dependence is stronger for rotation about the twofold axis, where the rotation pattern exhibits a periodic symmetry π. We introduce a model that we name as "stacked planar," which reproduces the orientation-dependent shape of the NMR spectra of the decagonal AlNiCo QC for rotation about the periodic axis, whereas—due to assumed amorphous order within the atomic planes—it does not yield orientation-dependent spectra for rotation about the quasiperiodic axis.

DOI: 10.1103/PhysRevB.71.014204 PACS number(s): 61.44.Br, 71.23.Ft, 76.60.−k

I. INTRODUCTION

Among the currently available thermodynamically stable quasicrystals (QCs), decagonal (*d*) quasicrystals are of high interest because they exhibit quasiperiodicity in a plane and periodicity in the orthogonal direction, thus representing two-dimensional (2D) QCs. This feature makes *d*-QCs especially attractive to study the effects of quasiperiodicity versus periodicity on the physical properties of solids, as the experiments can be performed on the same sample along different (periodic and quasiperiodic) crystallographic directions. A convenient experimental technique that probes the physical properties of the material on a local atomic level is the nuclear magnetic resonance (NMR) spectroscopy. NMR provides information about (i) local atomic environments through the nuclear electric quadrupole interaction with the surrounding electric charges; (ii) local electronic and magnetic structure through the magnetic hyperfine electron-nucleus interactions; and (iii) excitations, fluctuations and diffusion of the atoms and electrons in the system through the nuclear spin-lattice and spin-spin relaxations. At present there exist many NMR studies of icosahedral (i) QCs[1–17] that are quasiperiodic in all three dimensions. The important results, relating to the quasiperiodicity, are (1) the presence of a wide distribution of electric-field-gradients (EFGs) consistent with a broad distribution of local atomic environments and (2) vanishing small Knight shifts and long spin-lattice relaxation, both compatible with an anomalously low density of states (DOS) of conduction electrons at the Fermi level E_F. Regarding the distribution of local atomic environments, ^{27}Al NMR line shape studies[1,13] of *i*-AlPdMn single-grain samples have demonstrated that the distribution of the EFG tensor orientations in a single grain is not much different from spherically isotropic, as found in a crystalline powder of a periodic material. However, a weak orientation dependence of the spectrum in a magnetic field was detected,[13] indicating that out of the broad, isotropic-like distribution of the EFG tensor orientations, some solid-angle directions are common to larger fraction of Al sites than others. In addition to the broad angular distribution of the EFG tensor orientations, a broad distribution of the EFG tensor eigen values was detected, too.[1]

Whereas the NMR investigations of *i*-QCs are numerous, the NMR studies of *d*-QCs are still scarce.[18,19] As *d*-QCs are quasiperiodic in 2D, one expects a similar broad distribution of the local atomic environments and the associated distributions of the EFG tensor orientations and magnitudes to apply to the quasiperiodic plane. Similarly to the *i*-QCs, this should result in a broad NMR spectrum that exhibits weak (or no) orientation dependence, when the external magnetic field is rotated within the quasiperiodic plane (or equivalently, the crystal is rotated about the quasiperiodic axis). The situation is different for rotation about an axis lying within the quasiperiodic plane (the periodic twofold axis), where the orientation of the quasiperiodic axis changes with respect to the magnetic field. Quite generally, in periodic crystals there exist usually a small number of different atomic environments, relating to the small number of physically nonequivalent lattice sites within the unit cell. Consequently, there exist a small number of different EFG tensors and the NMR spectrum of a periodic system consists of one or several narrow lines that exhibit orientation dependence.

It is the purpose of this paper to investigate the effect of quasiperiodicity versus periodicity on the NMR spectra of decagonal QCs by studying orientation dependence of the

^{27}Al NMR spectrum of a *d*-AlNiCo single-grain QC around the quasiperiodic and periodic directions. We give first a theoretical consideration of the NMR spectrum and then analyze the experimental spectra by resolving the electric and magnetic contributions to the line shape and width. The ^{27}Al spin-lattice relaxation rate is presented also.

II. THEORETICAL NMR LINE SHAPE

We derive a theoretical ^{27}Al NMR line shape of a nonmagnetic QC (like the *d*-AlNiCo) by discussing first the electric and magnetic interactions of the ^{27}Al nucleus (spin $I=5/2$) with the surrounding ions and electrons in the quasiperiodic lattice. The NMR resonance frequency corresponding to the $m\rightarrow m-1$ spin transition of the *i*th ^{27}Al nucleus can be written as a sum[20,1]

$$\nu_i(m)-\nu_0=\nu^{(1)}_{quad,i}(m)+\nu^{(2)}_{quad,i}(1/2)+\nu_{mag,i}, \tag{1}$$

where $\nu_0=\gamma_n B_0/2\pi$ is the Zeeman frequency and γ_n is the nuclear gyromagnetic ratio. The term $\nu^{(1)}_{quad,i}(m)$ is the first-order quadrupole shift that affects any spin transition $m\rightarrow m-1$, except the central $(1/2\rightarrow -1/2)$ one

$$\nu^{(1)}_{quad,i}(m)=-\frac{\nu_{Q,i}}{2}\left(m-\frac{1}{2}\right)(3\cos^2\theta_i-1+\eta_i\sin^2\theta_i\cos 2\phi_i). \tag{2}$$

The quadrupole coupling constant $\nu_{Q,i}=3e^2q^{(i)}Q/20h$ is determined by the largest principal value of the EFG tensor at the lattice site *i*, which can be written as[20]

$$eq^{(i)}=V^{(i)}_{ZZ}=V^{ion}_{ZZ,i}(1-\gamma^{(i)}_{\infty})+V^{el}_{ZZ,i}. \tag{3}$$

The first term on the right of Eq. (3) originates from the neighboring ionic charges, enhanced by the Sternheimer antishielding factor $1-\gamma^{(i)}_{\infty}$ due to the ionic electric field polarization of the core electrons, whereas the second term originates from the charges of the conduction electrons. The angles θ_i and ϕ_i in Eq. (2) describe the orientation of the applied magnetic field with respect to the principal-axes system (PAS) of the EFG tensor, and $\eta_i=(V^{(i)}_{XX}-V^{(i)}_{YY})/V^{(i)}_{ZZ}$ is the quadrupole asymmetry parameter. The first-order quadrupole shift is independent of the external magnetic field.

The second-order quadrupolar shift is important only for the central transition, which is not affected by the quadrupolar interaction in first order. It is inversely proportional to the external magnetic field and is written as

$$\begin{aligned}\nu^{(2)}_{quad,i}(1/2)=\frac{\nu^2_{Q,i}}{12\nu_0}[&6\sin^2\theta_i(1-9\cos^2\theta_i)\\&-4\eta_i\cos 2\phi_i\sin^2\theta_i(9\cos^2\theta_i+1)\\&+\eta_i^2(-16/3+8\cos^2\theta_i+6\cos^2 2\phi_i\sin^4\theta_i)].\end{aligned} \tag{4}$$

The term $\nu_{mag,i}$ in Eq. (1) represents the frequency shift due to the magnetic hyperfine coupling between the nuclear spins and the *s*, *p*, and *d* conduction electrons. This shift is the same for all nuclear spin transitions and is linearly proportional to the external field

$$\nu_{mag,i}=\frac{\gamma}{2\pi}\left[K_i+\frac{K_{Z,i}}{2}(3\cos^2\theta_i-1+\epsilon_i\sin^2\theta_i\cos 2\phi_i)\right]H_0. \tag{5}$$

Here K_i is the isotropic Knight shift due to the contact interaction between the nucleus and the *s* electrons, whereas the parameters $K_{Z,i}$ and $\epsilon_i=(K_{X,i}-K_{Y,i})/K_{Z,i}$ are the largest eigenvalue and the asymmetry parameter of the traceless anisotropic Knight shift tensor that includes the dipolar interaction between the nucleus and the conduction electrons. Since the PASs of both tensors, the anisotropic Knight shift and the EFG, are determined by the local site symmetry of the nuclear site, we assume that they have the same orientation.

The lack of translational periodicity in the QC lattice introduces wide distribution of different local chemical environments, so that each nuclear site has in principle its own set of the $eq^{(i)}$, η_i, K_i, $K_{Z,i}$, ϵ_i, θ_i, and ϕ_i parameters. The distribution of these parameters causes an inhomogeneous broadening of the NMR spectrum, whereas their mean values shift its center of gravity. To obtain the spectrum $I(\nu)$ of a single-grain sample, we first integrate the frequency of each $m\rightarrow m-1$ transition over the distribution function *g* of these parameters. We get

$$F(m)=\int \nu(m)g(eq,\eta,K,K_Z,\epsilon,\theta,\phi)d\Omega, \tag{6}$$

where $d\Omega$ is a differential of the phase space spanned by all the parameters in the distribution. For polygrain and powder samples one has to perform also the powder average over the random orientation of the grains. The spectrum is finally obtained by summing up all $F(m)$ contributions, weighted by their respective amplitudes of the nuclear spin transitions $\beta_m=I(I+1)-m(m-1)$:

$$I(\nu)=\sum_{m=5/2}^{-3/2}\beta_m F(m). \tag{7}$$

The shape of the NMR spectrum, given by Eq. (7), depends crucially on the shape of the multiparameter distribution function *g* that contains parameters pertinent to both, the electric quadrupole and the magnetic hyperfine interactions. In view of the very large ^{27}Al quadrupole coupling constants $\nu_Q\approx 2$ MHz and anomalously small isotropic Knight shifts of 100–200 ppm found in Al-based *i*-QCs,[1] we can make the following simplification. We assume that the magnetic shift of the spectrum can be described by a small uniform shift *K* (describing the isotropic Knight shift). The anisotropic Knight shift, which produces inhomogeneous broadening, is of the same order as the isotropic shift and can therefore be to a first approximation neglected,[1] when compared to the quadrupolar broadening (for our *d*-AlNiCo sample, this will be proven also from the field dependence of the line broadening). Within this approximation, the number of parameters in the distribution function *g* is reduced to 4, so that $g(eq,\eta,\theta,\phi)$ depends only on the parameters characterizing the EFG tensor magnitude and orientation.

In the experimental section we shall show that the ^{27}Al NMR spectra of the *d*-AlNiCo exhibit orientation dependence in the magnetic field. In an attempt to reproduce theoretically the orientation-dependent ^{27}Al line shapes using Eq. (7), we introduce a numerical model of the EFG distribution function $g(eq, \eta, \theta, \phi)$, which contains structural features specific to 2D QCs like the layer structure and the twofold symmetry in the periodic domain. In the following we describe this model and show that it reproduces well the NMR spectra in an orientation-dependent manner.

The orientation dependence of the quadrupole-perturbed NMR spectra in the magnetic field is related to the distribution of the EFG tensor PAS orientations and, hence, to the multiplicity of nonequivalent ^{27}Al sites. For a single-grain sample, the sum over the θ, ϕ angles runs over a finite number of discrete values, corresponding to different orientations of the EFG PASs at nonequivalent sites. The NMR spectrum exhibits orientation dependence only if there exists a local orientation of the PAS common to a large fraction of Al sites of the single grain, i.e., not all solid-angle directions occur with equal probability. In the case of no preferential solid angle, the spectrum is orientation independent. The EFG distribution in nonmagnetic aperiodic solids, such as glasses, nanostructured materials, and icosahedral QCs, has been investigated by Czjzek *et al.*[21] using a spherical shell model of dense random packing of hard spheres and a point-charge calculation. Le Caër and Brand[22] later introduced a model directly related to the model of Czjzek *et al.*, which they called the Gaussian isotropic model (GIM) and showed that GIM represents the limiting case for many different models with a large number of independent contributions to the EFG tensor, which is not restricted to a point-charge model. The GIM was successfully applied to extract the EFG tensor distribution from Mössbauer spectra of Fe-doped *i*-Al-Si-Mn(Cr) QCs.[23] Our model is directly related to the GIM, but with an important difference. While in the GIM, the atoms are randomly packed in spherical shells, hence yielding a structure that is amorphous and spherically isotropic on the average in three-dimensional (3D) (yielding no orientation dependence of the NMR spectra), we assume in our model that atoms are randomly packed in equidistant parallel planes, thus representing layered structure, which is amorphous in a plane, but represents a one-dimensional (1D) periodic crystal in the orthogonal direction. These ideas follow the structural model of the *d*-AlNiCo by Burkov,[24] which describes its structure as a stack of two (x,y) plane layers per orthogonal (z) period. Each layer exhibits only fivefold symmetry, but the layer at $z=c/2$ is rotated by 36° with respect to the layer at $z=0$, revealing overall decagonal symmetry. In our case, the atomic order within each layer is amorphous, so that the tenfold symmetry is not present and the model cannot give orientation-dependent NMR spectra for the crystal rotation around the axis perpendicular to the planes (corresponding to the tenfold axis of the *d*-AlNiCo). The model, however, yields orientation dependence for the rotation about an axis lying within the plane (the twofold axis). From this point of view, the model is not restricted to decagonal QCs only, but should be applicable also to other 2D QCs like those of pentagonal, octagonal, and dodecagonal symmetry.

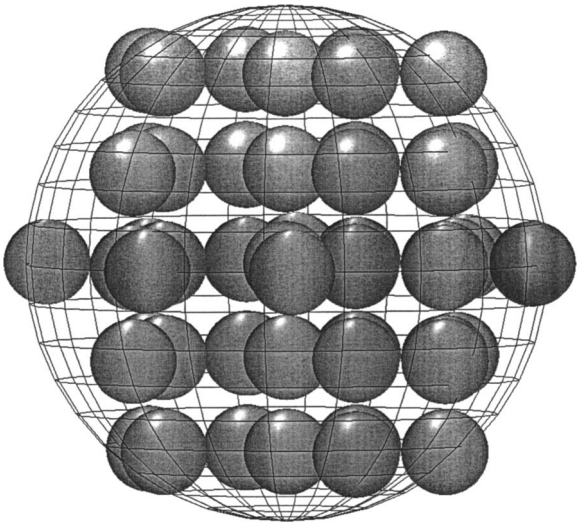

FIG. 1. Atomic structure used in the stacked-planar model for the calculation of the NMR spectrum of 2D QCs. The layers are periodically stacked along one direction, whereas the atomic order within the layers is amorphous. The sphere denotes the volume within which charges are taken into account for the calculation of the EFG in the sphere center.

The calculation of the EFG distribution proceeds as follows. A basic atomic layer is constructed by a random generation procedure, where hard spheres of radius R_{ion} and of random charge $\pm q$ are placed at random in the (x,y) plane of the crystal-fixed coordinate system, so that a densely packed 2D amorphous structure (the spheres may touch) is obtained. The *same* layer is then equidistantly stacked along the z axis of the crystal frame, providing translational symmetry in that direction. The distance D between planes is a variation parameter, which is always very close to $D=2R_{ion}$ (when layers are touching). In the next step, a sphere of radius $6R_{ion}$ is drawn (Fig. 1) and the EFG tensor elements are calculated in the sphere center (which coincides with the center of one of the atoms) in the crystal-fixed frame by a point charge calculation from the charges within the sphere. Because of the mirror symmetry of the model [the atomic (x,y) plane is a mirror plane], only four EFG elements are different from zero in the crystal frame (the three diagonal ones plus the V_{xy} term), with only three being independent. The EFG tensor is then transformed into the laboratory frame (x',y',z'), chosen to have its z'-axis parallel to the external magnetic field B, where it is diagonalized into its PAS [denoted as (X,Y,Z)] and the eigenvalues are labeled in the usual way as $|V_{XX}| \leq |V_{YY}| \leq |V_{ZZ}|$. The eigenvalue parameters $V_{ZZ}=eq$ and η are then put into histograms. The same procedure in now repeated 2×10^5 times, each time with a new randomly generated basic atomic layer, so that complete histograms for the distributions $f(V_{ZZ})$ and $r(\eta)$ are obtained. The parameters V_{ZZ} and η are in fact distributed by a single joint distribution $F(V_{ZZ},\eta)$, so that $f(V_{ZZ})=\int_0^1 F(V_{ZZ},\eta)d\eta$ and $r(\eta)=\int_{-\infty}^{+\infty} F(V_{ZZ},\eta)dV_{ZZ}$ represent two marginal distributions[21] of $F(V_{ZZ},\eta)$. In order to calculate a twofold rotation pattern of the orientation-dependent NMR spectra in a magnetic field, we choose initially the crystal-(x,y,z) and the laboratory

(x',y',z') frames to coincide and then rotate the crystal frame about the x' axis (that coincides with x), with β denoting the rotation angle. Finally, we mention that in the case where the atoms are placed into spherical shells instead into 2D planes, our calculation recovers fully the results of Czjzek *et al.*[21] (see their Fig. 2) and the GIM model (see Fig. 1 of Le Caër and Brand[22]), for which the two marginal distributions $f(V_{ZZ})$ and $r(\eta)$ are analytically known [given by, e.g., Eqs. (15) and (16) of Ref. 22). Our model can, therefore, be considered as an extension of the spherically isotropic models to stacked planar structures and for that reason we refer to it as the stacked-planar model in the following.

III. EXPERIMENT

The experiment was performed on a decagonal $Al_{72.6}Ni_{10.5}Co_{16.9}$ single-grain QC (in the following referred to as *d*-$AlNiCo_{16.9}$), grown by the self-flux technique. The crystal exhibited decagonal-prismatic growth morphology with clear facets, arranging perpendicular to the tenfold direction. The material was in a basic-cobalt (*b*-Co) decagonal modification, showing no inclusions and precipitations of secondary phases. The details of its preparation and characterization were published elsewhere.[25] Here we mention that the same sample was used before in an ^{27}Al NMR study of atomic motion.[18]

Due to strong inhomogeneous broadening, NMR absorption spectra of QCs extend over a frequency interval of many megahertz, which is much too broad to be detected by a standard NMR spectrometer (of typical bandwidth about 300 kHz). Therefore, special techniques of magnetic field sweep and frequency sweep have to be applied to record a quasicrystalline spectrum. In order to resolve the spectrum on its electric quadrupole and magnetic contributions, one has to perform experiments in different magnetic fields. For that purpose we used two experimental setups. In the first one, we used a custom two-coil superconducting magnet Oxford, where the center field $B_0=2.35$ T is provided by the main coil and the secondary coil is used for the field-sweep purpose in the range ±10% around the central value. The field was changed in steps (typically 5–10 G) and the spin-echo intensity was recorded as a function of the field strength by irradiating at a constant frequency ($\nu_0=26.134$ MHz), chosen to coincide with the ^{27}Al central transition. One half of the echo was Fourier transformed (FT) and the spectral intensity was integrated in a narrow frequency interval of 10 kHz (less than one field step) around the center irradiation frequency. The sweep coil was put into the persistent mode after each step, assuring high stability of the field during the measurements. In the second setup, the spectra were recorded by a frequency-sweep technique in a constant field $B_0=6.34$ T (corresponding to the ^{27}Al Larmor frequency of 70.35 MHz), with the total sweep range of 11 MHz. A typical frequency step was 10–50 kHz and the half-echo FT spectra were again integrated in an interval of 10 kHz. The NMR probe head was tuned automatically via a stepper-motor system. In both experimental setups (field- and frequency-sweep experiments), the sweep range was large enough to record both, the ^{27}Al and the ^{59}Co NMR spectra in a single run. A two-pulse Hahn-echo sequence was used with a $\pi/2$ pulse length of 2 μs.

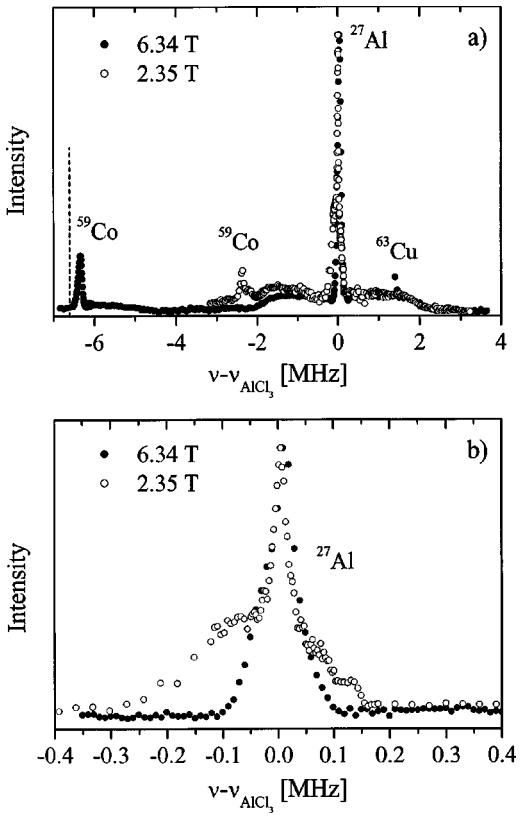

FIG. 2. (a) The NMR spectra of the *d*-$AlNiCo_{16.9}$ at $T=50$ K for the crystal orientation ten-axis perpendicular to the field (PRP orientation). Solid circles represent the frequency-swept spectrum in a field 6.34 T (the high-field spectrum), whereas open circles represent the field-swept spectrum for the center field 2.35 T (the low-field spectrum). The origin of the frequency scale is taken at the ^{27}Al resonance frequency of the $AlCl_3$ aqueous solution. The ^{63}Cu resonance originates from the copper in the probe head. The dashed vertical line marks the ^{59}Co Larmor frequency in the field 6.34 T. (b) ^{27}Al central lines in the two magnetic fields on an expanded frequency scale.

IV. RESULTS AND DISCUSSION

A. The NMR spectrum

The NMR spectra of the *d*-$AlNiCo_{16.9}$ for the crystal orientation ten-axis perpendicular to the field (in the following referred to as the "perpendicular" or PRP orientation) taken at two magnetic fields are displayed in Fig. 2(a). Solid circles represent the frequency-swept spectrum in a field 6.34 T (in the following referred to as the "high-field" spectrum), whereas open circles represent the field-swept spectrum for the center field 2.35 T (the "low-field" spectrum). In both cases the origin of the frequency scale is taken at the ^{27}Al resonance frequency of the $AlCl_3$ aqueous solution. Three resonances are observed in the spectrum: ^{27}Al, ^{59}Co, and ^{63}Cu, where the last resonance originates from the copper in the probe head. The high-field spectrum can be recognized by having larger separation between the ^{27}Al and ^{59}Co reso-

nances. The ^{27}Al ($I=5/2$) spectrum exhibits a structure of a broad "background" line, corresponding to the first-order quadrupole-perturbed $\pm 5/2 \leftrightarrow \pm 3/2$ and $\pm 3/2 \leftrightarrow \pm 1/2$ satellite transitions and the narrow, high-intensity line in the middle is the central line ($1/2 \leftrightarrow -1/2$), quadrupole perturbed in second order. A related structure applies also to the ^{59}Co ($I=7/2$) spectrum (note that the available frequency sweep width was not large enough to record the full satellite intensity on the negative side of the ^{59}Co central line). The fact that the ^{59}Co central line is shifted only by +200 kHz from its Larmor frequency $\nu_0(^{59}\mathrm{Co})=63.76$ MHz [shown by a dashed line in Fig. 2(a)] demonstrates that cobalt is in a nonmagnetic state. The electric-quadrupole origin of the large inhomogeneous broadening of the satellites is evident from its field independence. This is best seen on the positive frequency side of the ^{27}Al central line, where the satellite intensities of the high- and low-field spectra perfectly match. On the negative side this is less evident, as the ^{59}Co and the ^{27}Al spectra partially overlap and their satellite intensities between both central lines are superimposed (this is more pronounced in the low field, where the two resonances are closer together). The ^{27}Al spectrum extends in total over the frequency interval of about 8 MHz. Since this corresponds to $4\nu_Q$, this gives an estimate of the quadrupole coupling constant $\nu_Q \approx 2$ MHz. This large ν_Q value indicates that the quadrupole broadening may be dominant also on the central line, which is quadrupole perturbed in second order only. The field dependence of the ^{27}Al central line displayed in Fig. 2(b) shows that this is indeed the case. The low-field central line extends over the frequency interval 450 kHz and is roughly 2.5 times broader than the high-field one that extends over 200 kHz. This is in agreement with the second-order quadrupolar broadening that is inversely proportional to the external magnetic field (recall that magnetic broadening increases linearly with the field). The factor of 2.5 is consistent with the ratio 2.7 of the magnetic fields.

B. The ^{27}Al Knight shift

The magnetic (Knight) shift of the spectrum may be determined on the central line, where it is not masked by the enormously large first-order quadrupole effect. Closer inspection of the spectra in Fig. 2(b) reveals that the peak of the ^{27}Al low-field central line is shifted by $\Delta\nu=\nu-\nu_{\mathrm{AlCl_3}}=4$ kHz relative to the $AlCl_3$ resonance, whereas the shift increases to 14 kHz in the high field. The frequency shift of the peak is thus very small as compared to the total width of the inhomogeneously broadened central line. This shift is a sum of the quadrupolar and the magnetic contributions and scales with the magnetic field as $\Delta\nu=a/B+bB$. Since $\Delta\nu$ is known at two fields, we can calculate the coefficients a and b, describing the second-order quadrupolar and the magnetic contributions, respectively. We get $a=-3.3$ kHz·T and $b=2.3$ kHz/T, which yields, for $B=2.35$ T, a second-order quadrupolar shift $a/B=-1.4$ kHz and a magnetic shift $bB=5.4$ kHz. In the high field $B=6.34$ T, the shifts become $a/B=-0.5$ kHz and $bB=14.5$ kHz. Here we emphasize that the shift $\Delta\nu$ was determined from the field- and frequency-swept spectra, where each point in the spectrum represents an integrated intensity in a window of 10 kHz. This represents a rather coarse sampling of the central line and the peak position was consequently determined by fitting the top of the central line by a bell function. The obtained shift values should be considered to have precision ±1 kHz. The temperature dependence of the shift in both fields is displayed in Fig. 3, where no temperature dependence is noticed between 300 and 4 K. Normalizing the magnetic shift to the resonance frequency $\nu_{\mathrm{AlCl_3}}$, the relative shift amounts $K=bB/\nu_{\mathrm{AlCl_3}}=(2.1\pm0.2)\times10^{-4}$, which we associate with the ^{27}Al isotropic Knight shift K of the d-$AlNiCo_{16.9}$. This value is of the same order as the K values found in icosahedral Al-based QCs like the AlCuFe(Ru) and AlPdMn (where K values between 1.6×10^{-4} and 2.6×10^{-4} were reported[1]) and is a factor 8 smaller than in the fcc Al (free-electronlike) metal, where $K_{\mathrm{Al}}=1.6\times10^{-3}$. Since the Knight shift is proportional to the electronic DOS at the Fermi level $g(E_F)$, we find that the DOS in the d-$AlNiCo_{16.9}$ is reduced with respect to the Al metal also by $g_{\mathrm{Al}}/g \approx K_{\mathrm{Al}}/K \approx 8$, thus by a very similar factor as in the icosahedral Al-based QCs. Regarding the anisotropic Knight shift, which produces inhomogeneous magnetic broadening that increases linearly with the field (in contrast to the isotropic Knight shift, which just shifts the resonance, but does not produce inhomogeneous broadening), the inverse-field dependence of the central lines observed in Fig. 2(b) with the proper scaling (the estimated spectrum width decrease for a factor 2.5 matches well to the ratio of the fields 2.7) demonstrates that the magnetic broadening is minute as compared to the quadrupolar broadening even on the central line. Therefore, the magnetic broadening due to anisotropic Knight shift can be, to a good approximation, neglected. This is in agreement with the results of the Knight shift study in icosahedral Al-based QCs,[1] where the anisotropic Knight shift was also found negligibly small.

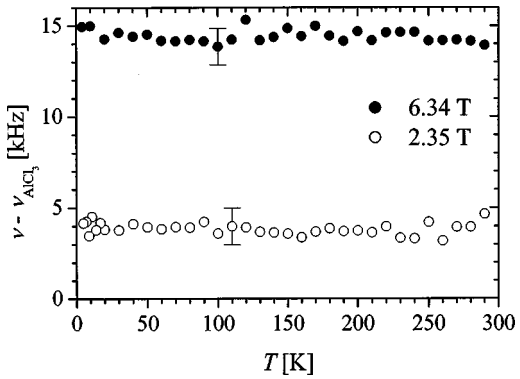

FIG. 3. Temperature-dependence of the shift of the ^{27}Al central line peak position (PRP orientation) relative to the $AlCl_3$ resonance between 300 and 4 K in two magnetic fields.

The DOS reduction g_{Al}/g and the ^{27}Al Knight shift K of the d-$AlNiCo_{16.9}$ can be estimated also from the ^{27}Al spin-lattice relaxation rate T_1^{-1}. The K and the T_1^{-1} values are related by the Korringa relation[26]

$$K^2 = \frac{\hbar}{4\pi k_B T_1 T}\left(\frac{\gamma_e}{\gamma_n}\right)^2, \tag{8}$$

where γ_e is the electronic gyromagnetic ratio, so that Eq. (8) is very useful for calculating an estimate for the relaxation

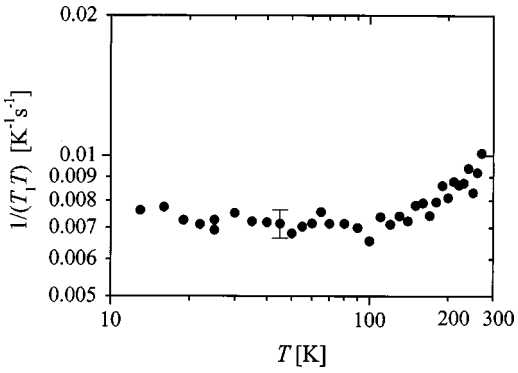

FIG. 4. Temperature-dependent ^{27}Al spin-lattice relaxation rate of the *d*-AlNiCo$_{16.9}$ in the field 6.34 T displayed in the $(T_1T)^{-1}$ vs. T plot.

rate knowing the value of the Knight shift and vice versa. The temperature-dependent ^{27}Al spin-lattice relaxation rate was measured in the interval from 300 to 10 K. The measurements were performed in the high field 6.34 T on the central line by irradiating at the frequency $\nu(^{27}\mathrm{Al}) = 70.35$ MHz. The saturation-recovery pulse sequence was employed with a saturation train of sixty $\pi/2$ pulses of 2 μs duration. The spin-lattice relaxation rate T_1^{-1} was extracted from the magnetization-recovery curves by the long-saturation magnetic relaxation model of Narath.[27]

The temperature-dependent ^{27}Al spin-lattice relaxation rate of the *d*-AlNiCo$_{16.9}$ is displayed in Fig. 4 in the form of a $(T_1T)^{-1}$ vs T plot, which yields for regular metals a horizontal $(T_1T)^{-1}$=const. line (the Korringa law). For the *d*-AlNiCo$_{16.9}$ we observe a $(T_1T)^{-1}$=const. plateau at temperatures below 150 K, whereas above that temperature $(T_1T)^{-1}$ starts to increase slightly. The plateau below 150 K demonstrates that the dominant spin-lattice relaxation mechanism there is via the conduction electrons, as in regular metals. The increase of the $(T_1T)^{-1}$ at higher temperatures was observed quite commonly in the *i*-QCs[6,8,9,12,14,16] but the origin of this enhanced relaxation is still ambiguous. Here we shall analyze only the $(T_1T)^{-1}$=const. part of the relaxation rate below 150 K, whose interpretation is clear. The quadratic dependence of the relaxation rate on the DOS, $(T_1T)^{-1} \propto g^2(E_F)$, allows estimating the reduction of $g(E_F)$ in the *d*-AlNiCo$_{16.9}$ relative to the Al metal. From Fig. 4 we find $(T_1T)_{\mathrm{AlNiCo}} = 135$ K s below 150 K, whereas for the fcc Al metal this product amounts[28] $(T_1T)_{\mathrm{Al}} = 1.88$ K s. From these values we estimate the DOS reduction to be $g_{\mathrm{Al}}/g \approx \sqrt{(T_1T)_{\mathrm{AlNiCo}}/(T_1T)_{\mathrm{Al}}} = 8.5$, in good agreement with the value obtained from the Knight shift analysis (where $g_{\mathrm{Al}}/g = 8$).

From the known Knight shift ($K = 2.1 \times 10^{-4}$) and the product $T_1T = 135$ K s we can test how these values fulfill the Korringa relation [Eq. (8)]. We obtain $K^2 = 4.4 \times 10^{-8}$ and $\hbar\gamma_e^2/(4\pi k_B T_1 T \gamma_n^2) = 2.9 \times 10^{-8}$, which may be considered as a very reasonable matching and gives confidence in the experimental values of the K and T_1T parameters.

C. Orientation-dependent ^{27}Al NMR spectra

The earlier results and conclusions are based on the experimental spectra taken at the PRP orientation of the monocrystal, i.e., where the magnetic field lies within the tenfold-symmetric quasiperiodic plane. Therefore, rotating the crystal for $2\pi/10$ about the tenfold axis should lead to a repetition of the situation and the NMR spectrum should exhibit no (or at most a weak) orientation dependence. The situation is different for the rotation of the crystal about an axis lying within the quasiperiodic plane (corresponding to the twofold axis of the *d*-AlNiCo structure), where the tenfold axis changes its orientation relative to the field. In Fig. 5 we display the frequency-swept (high-field) NMR spectra at 200 and 10 K at two orientations: (a) PRP orientation (ten-axis perpendicular to the field) and (b) parallel or PLL orientation (ten-axis parallel to the field). The ^{27}Al line shapes at the two orientations exhibit pronounced differences. While the satellite part of the PRP spectrum shows a more or less featureless shape, the satellite part of the PLL spectrum exhibits clearly developed sharp features. Regarding the temperature dependence of the spectra, no noticeable temperature-dependent changes (except for the trivial decrease in noise at low temperatures) in the line shape, peak position and line width were observed between room temperature and 10 K at any of the two orientations. Here it is also worth noting that the temperature-independent position of the ^{59}Co central line in Fig. 5 is another indication of the nonmagnetic character of cobalt atoms (in the case of paramagnetism the shift should go as $\Delta\nu \propto 1/T$).

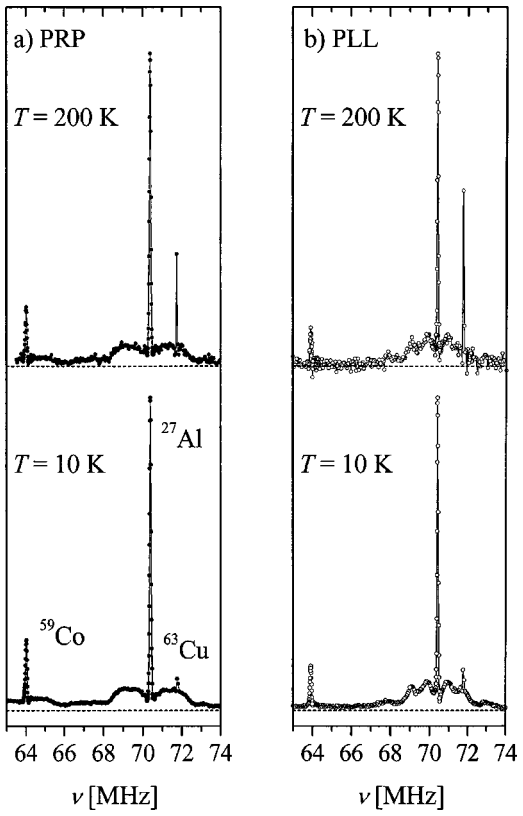

FIG. 5. The frequency-swept (high-field) NMR spectra of the *d*-AlNiCo$_{16.9}$ at 200 and 10 K taken at two orientations: (a) PRP orientation (ten-axis perpendicular to the field) and (b) PLL orientation (ten-axis parallel to the field).

The orientation-dependent ^{27}Al NMR spectra of the *d*-AlNiCo$_{16.9}$ single grain for rotations about the quasiperi-

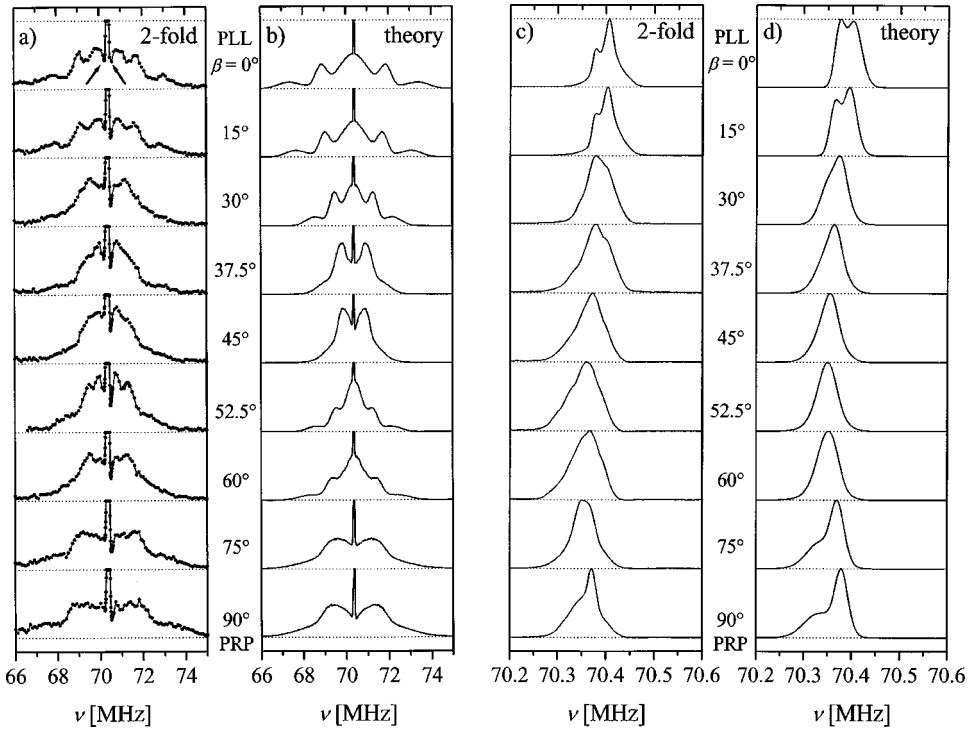

FIG. 6. Orientation-dependent ^{27}Al high-field NMR spectra at 80 K of the d-$AlNiCo_{16.9}$ single-grain sample for rotation about the twofold axis. In (a), the frequency-swept rotation pattern is shown on an expanded vertical scale, so that the satellite intensity is clearly visible, whereas the central line is clipped on this scale. In (b), the corresponding theoretical rotation pattern, obtained by the stacked-planar model, is displayed. The two sharp dips, located on both sides of the central line [marked by arrows on the $\beta=0$ spectrum of (a)] are artifacts of the frequency-sweep technique, occurring at the transition from the narrow central line to the broad satellite intensity. The experimental central lines, obtained by the FT technique (see text) are displayed in (c), whereas the theoretical lines are shown in (d). $\beta=0$ corresponds to the PLL orientation and $\beta=90°$ to the PRP orientation.

odic and periodic directions were studied by the frequency-sweep technique in the high field (6.34 T) at $T=80$ K. In the rotation about the quasiperiodic tenfold axis, the shape of the spectrum was found equal to that of the PRP spectrum shown in Fig. 5(a) in the whole rotation pattern 0°–180°, with no noticeable orientation dependence within the accuracy of the frequency-sweep experiment. As discussed earlier, this is not surprising due to high (tenfold) symmetry of the crystal structure. The situation is different for the rotation about the periodic twofold axis. The twofold rotation pattern is shown in Figs. 6(a)–6(d), where the orientation $\beta=0$ corresponds to the PLL orientation and $\beta=90°$ to the PRP orientation. Since the spectra were found mirror symmetric around $\beta=90°$, only half of the rotation pattern (0°–90°) is displayed. In Fig. 6(a) the experimental spectra are shown on an expanded vertical scale, so that the orientation-dependent structure of the satellite intensity is clearly visible, whereas the central line is clipped on this scale and will be discussed separately. The rotation pattern exhibits quite strong orientation dependence; while the satellite intensity is in all cases continuous, it exhibits angular-dependent shape and fine structure. Here we mention that the two sharp dips, located on both sides of the central line [marked by arrows on the $\beta=0$ spectrum of Fig. 6(a)] are artifacts of the frequency-sweep technique, occurring at the transition from the narrow central line to the broad satellite intensity.

In Fig. 6(c), the twofold rotation pattern of the central line is displayed. As this line is narrow, the sampling by the frequency-sweep technique is too coarse to give details of its fine structure. For that reason we repeated the experiment, using this time a simpler method of FT of one half of the echo by irradiating at a fixed frequency corresponding to the peak position of the central line. The so-obtained FT-central lines were less than 10% narrower than the ones obtained with the frequency-sweep technique, showing that, in the high field, the FT spectra can be used quite reliably to study the central line shape. The advantage of the FT technique is a better digital resolution of the spectrum (finer sampling of the line), so that sharp details in the spectrum remain visible. The twofold rotation pattern from Fig. 6(c) again exhibits quite pronounced angle-dependent changes in the shape, width and fine structure of the central line.

The theoretical line shapes, calculated from the stacked-planar model, are displayed in Figs. 6(b) and 6(d) side by side to the experimental spectra. In Fig. 6(b) the theoretical spectra may be compared to the experimental satellite lines from Fig. 6(a). At practically all orientations the agreement is satisfactory, reproducing well both the overall shape and the fine structure of the satellite line. The discrepancy is in most cases related to the relative intensities of the fine details in the spectrum. The stacked-planar model correctly reproduces the broad featureless shape at the PRP ($\beta=90°$) orientation that transforms upon rotation into a narrower spectrum at $\beta=45°$ and finally to a broader spectrum with fine structure at the PLL ($\beta=0$) orientation. Here we emphasize that, in the calculation of the rotation pattern, we changed only the di-

rection of the magnetic field, with all other parameters being the same throughout the calculation. It is remarkable that our structural model, which exhibits translational periodicity in one dimension, but amorphous disorder instead of quasiperiodic order within the atomic planes, reproduces so well the experimental spectra of a real *d*-QC single-grain sample. The reason for this agreement could also be the presence of chemical and phason disorders on the quasiperiodic lattice.

The theoretical orientation-dependent central lines are displayed in Fig. 6(d) together with the experimental lines in Fig. 6(c). Also there the agreement between the theoretical and experimental lines is in most cases good, except for the mismatch of the relative intensities of the fine details in the spectra. For example, the theoretical and experimental lines at $\beta=0$ both exhibit a two-peak structure, but their theoretical intensity ratio is considerably different from that found experimentally. Nevertheless, the theoretical spectra reproduce reasonably well the orientation-dependent transformation of the spectrum from a narrow peak with a broad shoulder at $\beta=90°$, to a featureless single line at $\beta=45°$, and finally to a two-peak structure at $\beta=0$. In the following we will show that the theoretical model reproduces satisfactorily also the orientation-dependent first moment M_1 (the center of gravity) of the central line, hence, the change of its position with the orientation. Here we also mention that the shape of the low-field frequency-sweep central line of Fig. 2(b) (at the PRP orientation), exhibiting an asymmetric structure of a narrow peak and a broad shoulder on the low-frequency side, matches well to the corresponding theoretical spectrum [the PRP line in Fig. 6(d)]. Regarding the asymmetric shape of the high-field central line in Fig. 2(b), its fine details are smeared due to the frequency-sweep scanning mode, so that the asymmetry is better observed on the corresponding (PRP) FT line in Fig. 6(c).

The theoretical spectra were calculated using the fit parameter $D/2R_{ion}=1.1$ (the ratio of the distance between two atomic planes and the atomic diameter). This parameter influences the shape of the NMR spectra quite significantly. The resulting two marginal distributions $f(V_{ZZ})$ and $r(\eta)$ are displayed by solid lines in Fig. 7. The corresponding theoretical distributions of the spherically isotropic model [Eqs. (15) and (16) of Ref. 22] are shown for comparison as dashed lines. Regarding the distribution of the asymmetry parameter $r(\eta)$ [Fig. 7(a)], the difference between the two models appears mainly at small η. While in the spherically isotropic model, the probability of finding an EFG with $\eta=0$ is zero; it becomes nonzero in the stacked-planar model. The average asymmetry parameter, $\langle\eta\rangle\approx 0.6$, is practically the same in both models. The distribution $f(V_{ZZ})$ is displayed in Fig. 7(b). The horizontal V_{ZZ} scale is taken dimensionless, so that it should be multiplied by a proper scaling factor in order to obtain matching between the widths of the theoretical and experimental NMR spectra. The distributions of the two models have their integrals normalized to 1 and are displayed so that the positions of their maxima coincide. Both models give qualitatively similar distributions, exhibiting two peaks at $\pm V_{ZZ}$. The peaks of the stacked-planar model are somewhat narrower than those of the spherically isotropic model.

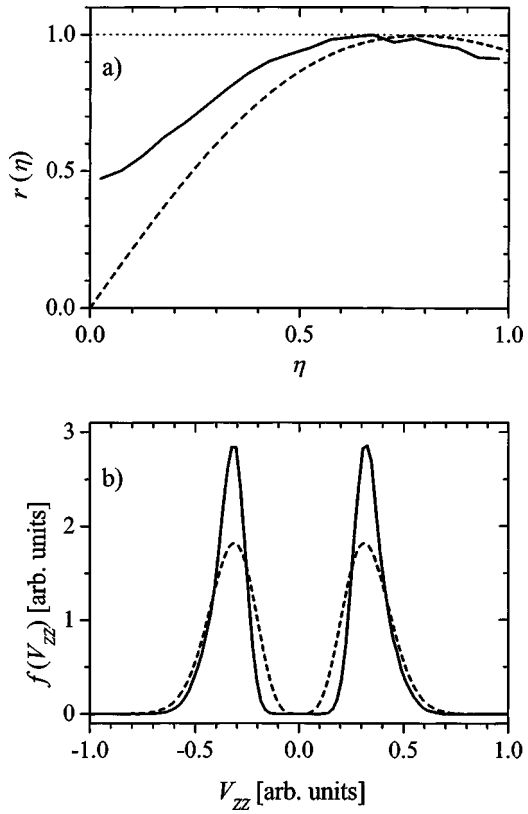

FIG. 7. Marginal distributions (a) $r(\eta)$ and (b) $f(V_{ZZ})$ (solid lines) used in the stacked-planar model to calculate the theoretical NMR spectra shown in Figs. 6(b) and 6(d). The corresponding theoretical distributions of the spherically isotropic model (see text) are shown for comparison as dashed lines. The $f(V_{ZZ})$ distributions have their integrals normalized to 1.

The origin of the orientation dependence of the NMR spectra can be understood from specific features of the stacked-planar model. Recall that this model is constructed by stacking the same randomly generated atomic layer along the periodic direction (corresponding to the ten-axis of the *d*-AlNiCo structure), so that all atoms lie on a mirror plane. Because of the mirror symmetry, the EFG PAS at every nuclear site has one of its axes directed along the periodic direction. Therefore, the nuclear sites can be divided into three groups: (a) those that have the EFG PAS *Z* axis along the periodic direction of the crystal (referred to as the G_Z-group sites), (b) those with the *Y* axis along the periodic direction (G_Y-group sites), and (c) those with the *X* axis along the periodic direction (G_X-group sites). From the *C*-infinity rotational symmetry of the atomic planes in the stacked-planar model (due to amorphous disorder within the planes) it follows that, for the G_Z group, the distribution of the *X* and *Y* principal axes is isotropic in the plane. The same isotropic distribution applies to the *Z* and *X* axes of the G_Y group and to the *Y* and *Z* axes of the G_X group. At the PLL orientation of the crystal with respect to the magnetic field ($\beta=0$), all G_Z-group sites have their *Z* axes parallel to the magnetic field, whereas the *Z* axes of the G_X- and G_Y-group sites are distributed isotropically within the planes, all making an angle 90° with respect to the magnetic field. This

anisotropic division of sites into three groups is at the origin of the orientation-dependence of the spectrum in a twofold rotation pattern.

The above analysis in terms of the three groups of sites, G_X, G_Y, and G_Z, is based on two specific symmetries of the stacked-planar model: (i) the mirror plane that coincides with the atomic planes and (ii) the *C*-infinity rotation axis perpendicular to the atomic planes. It is interesting to consider how these symmetries relate to the actual symmetry of the *d*-AlNiCo QC. According to Burkov,[24] the space group of *d*-AlNiCo is $P10_5/mmc$ (centrosymmetric), which contains a 10_5-screw axis perpendicular to the atomic layers and a mirror plane coinciding with the layers. While the mirror plane is present in both the *d*-AlNiCo and the stacked-planar model, the 10_5-axis of the *d*-AlNiCo is replaced by the *C*-infinity axis in the stacked-planar model. The success of the stacked-planar model in reproducing the NMR spectra of the *d*-$AlNiCo_{16.9}$ may be due to the existence of chemical and phason disorders in real *d*-AlNiCo samples,[29–31] which locally break the tenfold symmetry, so that *C*-infinity symmetry can be considered as a far approximation to the 10_5-screw axis.

D. Orientation-dependent first moment M_1 of the ^{27}Al central line

In the measurement of the orientation-dependent ^{27}Al NMR spectra of the *d*-$AlNiCo_{16.9}$ for rotation about the quasiperiodic tenfold axis, coarse sampling of the line inherent to the frequency-sweep technique and rather coarse angular resolution performed mostly in steps of 15° (due to time-consuming experiments) did not reveal any orientation dependence of the satellite spectra within the precision of the frequency-sweep technique. As for this rotation the physical situation in the crystal repeats every 36°, finer angular and better frequency resolutions of the spectra are needed to check for the possible orientation dependence of the spectra in the tenfold rotation pattern. Such improved-resolution experiments could be performed on the central line in the high field, using the FT spectra. For that reason we have remeasured the rotation patterns of the central line about the tenfold and twofold directions at room temperature with the FT technique and improved angular resolution of 7.5°. A collection of the ^{27}Al central lines for the tenfold rotation is displayed in Fig. 8(a), whereas the twofold rotation pattern is shown in Fig. 8(b) (note that this twofold pattern was obtained at room temperature whereas the one shown in Fig. 6(c) was collected at 80 K—wherefrom its better signal-to-noise). The position of the reference ν_{AlCl_3} frequency (70.35 MHz) is given as a dashed line. In both patterns we observe orientation dependence of the spectra, which is much more pronounced for the rotation about the twofold axis. For the tenfold rotation, the shape of the central line shows asymmetry toward the low-frequency side with additional hump that is more pronounced at some orientations, whereas the position of the line is mostly unchanged. Closer inspection of the spectra shows that the repetition of the line shape occurs five times between 0° and 180°. This is also evident from the angular dependence of the center of gravity

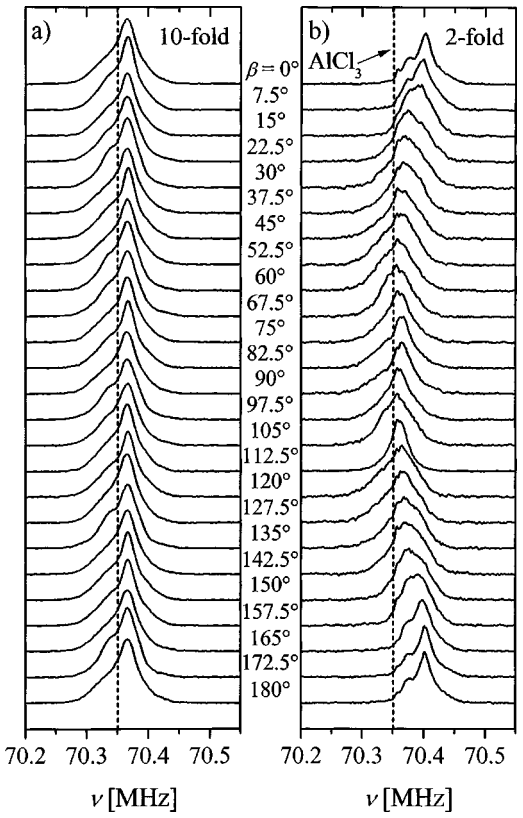

FIG. 8. Rotation patterns of the ^{27}Al central line obtained with the FT technique in the high field (6.34 T) at room temperature for the rotation about (a) the tenfold axis and (b) the twofold axis. The position of the reference ν_{AlCl_3} frequency (70.35 MHz) is shown by a dashed line.

of the spectrum (the first moment M_1, measured here relative to ν_{AlCl_3}), which is displayed in Fig. 9(a). For the tenfold rotation, the quasiperiodic symmetry of $\pi/5$ in the angular dependence of M_1 is clearly visible, though the total variation of M_1 is very small (about 2 kHz) as compared to the total central linewidth (150 kHz). The angular dependence is of the type $M_1 = a_1 + a_2 \sin 10\beta$ with $a_1 = 7.5$ kHz and $a_2 = 0.7$ kHz [solid line in Fig. 9(a)]. For the rotation about the twofold axis, the orientation dependence of the central line is much stronger. The structure and the position of the line both change significantly with the angle β, which is reflected in the angular dependence of M_1 [Fig. 9(b)]. This angular dependence is of the type $M_1 = b_1 + b_2 \cos 2\beta + b_3 \cos 4\beta$ with the periodic symmetry π, where the $\cos 4\beta$ term is characteristic of the second-order quadrupolar shift in a monocrystal.[32] M_1 is the largest for the PLL orientation and its total variation for the twofold rotation is 40 kHz, which is again considerably smaller than the total width of the central line. The fit [solid line in Fig. 9(b)] yielded $b_1 = 19.9$ kHz, $b_2 = 20$ kHz, and $b_3 = 7.2$ kHz. The orientation-dependence of the first moment of the central line for the twofold rotation was reproduced also theoretically by calculating M_1 from the numerically simulated spectra displayed in Fig. 6(d). It is observed [dashed line in Fig. 9(b)] that the stacked-planar model gives a qualitative agreement with the experiment.

The higher-precision rotation patterns of the central line displayed in Figs. 8(a) and 8(b) thus show that the spectra

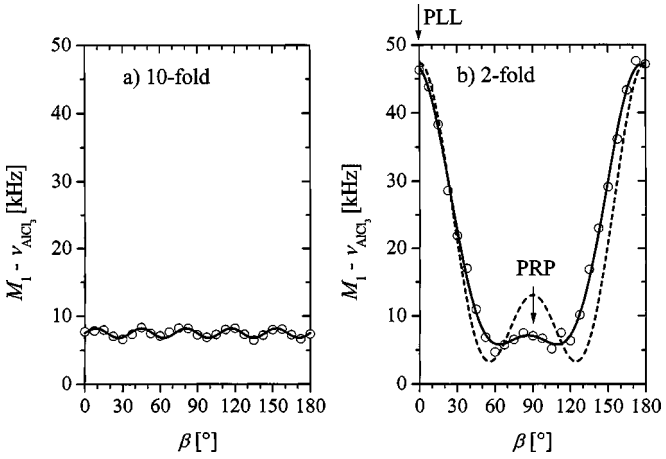

FIG. 9. Angular dependence of the center of gravity (the first moment M_1) relative to ν_{AlCl_3} of the ^{27}Al central lines from Fig. 8. (a) Rotation about the tenfold axis, where the solid line represents the fit with $M_1 = a_1 + a_2 \sin 10\beta$; (b) rotation about the twofold axis with the fit (solid line) $M_1 = b_1 + b_2 \cos 2\beta + b_3 \cos 4\beta$, whereas dashed line was obtained by calculating M_1 from the theoretical lines of the stacked-planar model displayed in Fig. 6(d). The nonperfect mirror symmetry of the experimental data in (b) across $\beta = 90°$ is due to slight misalignment (few degrees) of the starting (PLL) orientation of the crystal in the magnetic field.

are orientation dependent for rotation about both the quasiperiodic and the periodic axis. While in the twofold rotation, the spectrum exhibits strong angular anisotropy, the anisotropy is very small—but still significant—for the tenfold rotation. This demonstrates that the stacked-planar model is a good starting approximation for the calculation of the NMR line shape of 2D QCs, but, as it does not yield orientation dependence for rotation about the quasiperiodic axis due to amorphous order within the 2D planes, it should be further improved in future by considering the actual quasiperiodic structure of the atomic planes (replacing amorphous order by, e.g., pentagonal Penrose tiling, octagonal Ammann-Beenker tiling, etc.). Such models will then be specific to particular quasiperiodic symmetries, while the presented stacked-planar model can be considered as an approximation to all 2D QCs.

V. CONCLUSIONS

The NMR spectra of the *d*-AlNiCo$_{16.9}$ exhibit very large inhomogeneous broadening, extending over frequency interval of many megahertz, so that field- and frequency-sweep techniques are necessary to record a spectrum. We detected both the spectra of ^{27}Al and ^{59}Co, but the analysis was concentrated on the ^{27}Al resonance. In order to resolve the electric quadrupole and the magnetic contributions to the line shape and position of the spectra, the experiments were performed in two magnetic fields, differing in strength by a factor 2.7. The strong inhomogeneous broadening of the ^{27}Al spectrum is of the electric-quadrupole origin, which is evident from the magnetic-field independence of the broadening of the satellite part of the spectrum and the inverse-field dependence of the broadening of the central line. The electric quadrupole broadening is the dominant source of broadening also on the central line, which is quadrupole perturbed in second order only. The isotropic ^{27}Al Knight shift was found to have the same anomalously low value of less than 200 ppm as in the icosahedral Al-based QCs, suggesting a similar reduction of the electronic DOS at the Fermi level by a factor about 8 with respect to the free-electron Al metal. The same reduction factor was obtained also from the ^{27}Al spin-lattice relaxation rate. The Knight shift was found temperature-independent in the investigated temperature range 300–4 K, whereas the quadrupolar broadening also does not exhibit temperature dependence. The fact that the ^{59}Co resonance is centered almost at its Larmor frequency and its frequency shift does not change with temperature shows that cobalt is in a nonmagnetic state.

Since *d*-AlNiCo is quasicrystalline in 2D and crystalline periodic in the third dimension, the spectra of a single-grain sample exhibit orientation dependence in a magnetic field. Rotation pattern about the ten-axis shows a tiny, but significant orientation dependence of the central line shape and its center of gravity M_1 with the quasiperiodic symmetry $\pi/5$, compatible with the tenfold symmetry of the quasiperiodic structure. The orientation dependence is much stronger for rotation about the twofold axis, where the rotation pattern exhibits a periodic symmetry π. For both rotations the total variation of M_1 is considerably smaller than the width of the inhomogeneously broadened central line. Regarding orientation dependence of the satellite part of the spectra, the twofold rotation pattern exhibits significant variations in the line shape, width, and fine structure, whereas such changes could not be detected within the resolution of the frequency-sweep technique in the tenfold rotation pattern. The twofold rotation pattern could be satisfactorily reproduced theoretically by the stacked-planar model.

The orientation-dependence of the NMR spectra demonstrates that, despite the large number of nonequivalent lattice sites in the *d*-AlNiCo, the distribution of orientations of the EFG tensors in a single grain is strongly anisotropic. Future theoretical studies of the NMR spectra with the stacked-planar model, where the amorphous order within the atomic planes will be replaced by regular, long-range ordered quasiperiodic atomic patterns, should give more specific information on the details of the local atomic environments corresponding to a given EFG PAS. The presented stacked-planar model has, however, efficiently reproduced the orientation-dependent NMR spectra of the decagonal AlNiCo QC for the rotation about the periodic axis. This model is not restricted to decagonal QCs, but is applicable more generally to all planar structures, including 2D QCs of pentagonal, octagonal, decagonal, and dodecagonal symmetry, which exhibit either quasiperiodicity or large-unit-cell periodicity in a plane and periodicity on the scale of few interatomic distances in the third dimension.

ACKNOWLEDGMENT

We thank M. Feuerbacher from Jülich for provision of the *d*-AlNiCo$_{16.9}$ sample.

[1] As a reference paper on NMR in icosahedral quasicrystals, see A. Shastri, F. Borsa, D. R. Torgeson, J. E. Shield, and A. I. Goldman, Phys. Rev. B **50**, 15 651 (1994), and references therein.
[2] C. Lee, D. White, B. H. Suits, P. A. Bancel, and P. A. Heiney, Phys. Rev. B **37**, 9053 (1988).
[3] F. Hippert, L. Kandel, Y. Calvayrac, and B. Dubost, Phys. Rev. Lett. **69**, 2086 (1992).
[4] T. Shinohara, A. P. Tsai, and T. Masumoto, Hyperfine Interact. **78**, 515 (1993).
[5] F. Hippert, R. A. Brand, J. Pelloth, and Y. Calvayrac, J. Phys.: Condens. Matter **6**, 11189 (1994).
[6] E. A. Hill, T. C. Chang, Y. Wu, S. J. Poon, F. S. Pierce, and Z. M. Stadnik, Phys. Rev. B **49**, 8615 (1994).
[7] A. Shastri, D. B. Baker, M. S. Conradi, F. Borsa, and D. R. Torgeson, Phys. Rev. B **52**, 12 681 (1995).
[8] J. L. Gavilano, B. Ambrosini, P. Vonlanthen, M. A. Chernikov, and H. R. Ott, Phys. Rev. Lett. **79**, 3058 (1997).
[9] X.-P. Tang, E. A. Hill, S. K. Wounell, S. J. Poon, and Y. Wu, Phys. Rev. Lett. **79**, 1070 (1997).
[10] J. Dolinšek, B. Ambrosini, P. Vonlanthen, J. L. Gavilano, M. A. Chernikov, and H. R. Ott, Phys. Rev. Lett. **81**, 3671 (1998).
[11] J. Dolinšek, T. Apih, M. Simsič, and J. M. Dubois, Phys. Rev. Lett. **82**, 572 (1999).
[12] T. Apih, O. Plyushch, M. Klanjšek, and J. Dolinšek, Phys. Rev. B **60**, 14 695 (1999).
[13] T. Apih, M. Klanjšek, D. Rau, and J. Dolinšek, Phys. Rev. B **61**, 11 213 (2000).
[14] J. Dolinšek, M. Klanjšek, T. Apih, A. Smontara, J. C. Lasjaunias, J. M. Dubois, and S. J. Poon, Phys. Rev. B **62**, 8862 (2000).
[15] J. Dolinšek, M. Klanjšek, T. Apih, J. L. Gavilano, K. Giannò, H. R. Ott, J. M. Dubois, and K. Urban, Phys. Rev. B **64**, 024203 (2001).
[16] J. Dolinšek and M. Klanjšek, Phys. Rev. B **63**, 134203 (2001).
[17] J. L. Gavilano, D. Rau, Sh. Mushkolaj, H. R. Ott, J. Dolinšek, and K. Urban, Phys. Rev. B **65**, 214202 (2002).
[18] J. Dolinšek, T. Apih, P. Jeglič, M. Feuerbacher, M. Calvo-Dahlborg, U. Dahlborg, and J. M. Dubois, Phys. Rev. B **65**, 212203 (2002).
[19] D. Rau, J. L. Gavilano, Sh. Mushkolaj, C. Beeli, M. A. Chernikov, and H. R. Ott, Phys. Rev. B **68**, 134204 (2003).
[20] See, e.g., J. Winter, *Magnetic Resonance in Metals* (Clarendon Press, Oxford, 1971), Chaps. II, IV, and V.
[21] G. Czjzek, J. Fink, F. Götz, H. Schmidt, J. M. D. Coey, J.-P. Rebouillat, and A. Liénard, Phys. Rev. B **23**, 2513 (1981).
[22] See, for a review, G. Le Caër and R. A. Brand, J. Phys.: Condens. Matter **10**, 10715 (1998).
[23] R. A. Brand, G. Le Caër, and J. M. Dubois, J. Phys.: Condens. Matter **2**, 6413 (1990).
[24] S. E. Burkov, Phys. Rev. Lett. **67**, 614 (1991).
[25] M. Feuerbacher, C. Thomas, and K. Urban, in *Quasicrystals*, edited by H.-R. Trebin (Wiley, Weinheim, 2003), p. 15.
[26] J. Winter, *Magnetic Resonance in Metals* (Clarendon Press, Oxford, 1971), p. 42.
[27] A. Narath, Phys. Rev. **162**, 320 (1967).
[28] J. J. Spokas and C. P. Slichter, Phys. Rev. **113**, 1462 (1959).
[29] Y. Yan, S. J. Pennycook, and A. P. Tsai, Phys. Rev. Lett. **81**, 5145 (1998).
[30] S. Ritsch, H.-U. Nissen, and C. Beeli, Phys. Rev. Lett. **76**, 2507 (1996).
[31] Y. Yan and S. J. Pennycook, Phys. Rev. Lett. **86**, 1542 (2001).
[32] G. M. Volkoff, Can. J. Phys. **31**, 820 (1953).